NJC

Accepted Manuscript

This is an *Accepted Manuscript*, which has been through the Royal Society of Chemistry peer review process and has been accepted for publication.

Accepted Manuscripts are published online shortly after acceptance, before technical editing, formatting and proof reading. Using this free service, authors can make their results available to the community, in citable form, before we publish the edited article. We will replace this *Accepted Manuscript* with the edited and formatted *Advance Article* as soon as it is available.

You can find more information about *Accepted Manuscripts* in the Information for Authors.

Please note that technical editing may introduce minor changes to the text and/or graphics, which may alter content. The journal's standard Terms & Conditions and the Ethical guidelines still apply. In no event shall the Royal Society of Chemistry be held responsible for any errors or omissions in this *Accepted Manuscript* or any consequences arising from the use of any information it contains.

ROYAL SOCIETY OF CHEMISTRY

www.rsc.org/njc

Fabrication Visible-light-driven Photocatalyst and Degradation for Tetracycline Based on Photoinduced Interfacial Charge Transfer of $SrTiO_3/Fe_2O_3$ Nanowires

*Chunbo Liu, Guoling Wu, Jibin Chen, Kai Huang, Weidong Shi**

School of Chemistry and Chemical Engineering, Jiangsu University, Xuefu Road 301, Zhenjiang, 212013, P. R. China.

*Corresponding author: Tel.: +86 511 8879 0187 fax. : +86 511 8879 1108

E-mail address: swd1978@ujs.edu.cn (W. Shi)

Abstract

In our work, a new visible-light-driven photocatalyst $SrTiO_3/Fe_2O_3$ was firstly prepared via using a simple two-step process: the hydrothermal process and electrospinning technique. The photocatalysts of Fe_2O_3 nanowires (about 200 nm in diameter) were modified with $SrTiO_3$ nanocubes (about 50 nm) photocatalysts based on photoinduced interfacial charge transfer (IFCT). The as-prepared $SrTiO_3/Fe_2O_3$ photocatalysts exhibit enhanced photocatalytic activity in degrading tetracycline (TC) over the corresponding single component under visible light irradiation. The efficient photocatalytic performance of the composites could ascribe to the enhancement of visible light absorption efficiency and the efficient electron transfer from the valence band of $SrTiO_3$ nanoparticles to Fe_2O_3 nanowires. This work shows a potential applications prospect for purifying TC pollution in the environmental waste water because of its high efficiency and stability.

Keywords: $SrTiO_3/Fe_2O_3$, interfacial charge transfer, photodegradation, tetracycline

Introduction

At the present, the abuse of antibiotics, especially tetracycline (TC), in the pharmaceutical therapies and agricultural husbandry have been becoming a serious environmental problem worldwide.[1-7] Due to posing serious threats to the ecosystem

and human health by inducing proliferation of multi-resistant bacterial strains, hence, it is an urgent task to develop efficient treatment technologies to remove antibiotics left in the ecological environment. A wide variety of technologies have been used to remove antibiotics, such as UV/H_2O_2 process, biodegradation, electrochemical methods, and photocatalysis.[8-10] With enough efficiency in decomposing TC, low cost and operation-simplicity, the photocatalytic degradation processes provide a good tool for mitigation of environmental questions and degradation of antibiotics.[11] Recently, unremitting efforts on the high-efficiency photocatalytic degradation of TC have made obvious achievements, just as the literature reported before. [12-14] However, most of them for applications in degrading TC are mainly driven by UV-light rather than visible-light, which greatly limits their application in terms of photocatalysis.[15-16] Therefore, new-type visible-light driven photocatalysts with high efficiency for TC degradation are still desired.

So far, the $SrTiO_3$ (STO) semiconductor is one of the renowned photocatalysts due to the low cost, simple preparation, nontoxicity and chemical stability, which make it an attractive photocatalyst material.[17] However, due to its large band gap (3.2 eV), STO does not absorb photons in the visible light region of the electromagnetic spectrum, which significantly reduces its solar energy conversion efficiency. Moreover, STO has a relatively high electron-hole recombination rate, which is not conducive to its photocatalytic activity.[18-20] In order to improve its solar energy conversion efficiency, strenuous efforts have been committed, such as transition metal doping, inorganic dye-sensitizing, noble metal deposition and coupling with other

semiconductors, which would push the absorption onset of STO toward longer wavelength.[21-25] Nevertheless, many of these approaches have drawbacks of increasing crystal deformations or introducing defects that act as recombination centers.[26] It is encouraging that using metal oxide particles deposited on the surface of STO forming composites to improve the photodegradation activity, such as Ag_3PO_4/STO, $BaTiO_3$/STO and STO/Fe_2O_3.[27-28] Iron oxide (Fe_2O_3), an n-type semiconductor, is another typical photocatalyst utilized in the field of photocatalysis. The band gap of Fe_2O_3 (2.3 eV) is much smaller than that of STO, which is capable of absorbing visible light photons. As STO, Fe_2O_3 is also cheap accessible, nontoxic and chemically stable material for photocatalytic reactions.[29]

Electrospinning has been served as a unique technique to prepare the fibres with continuous morphology and tunable compositions in consideration of its high efficiency and low consumption. For years, incorporating functional nanoparticles (NPs) with electrospun fibres (NPs/electrospun) show great potential applications, flexibility in design of the channel material, efficient modulation of carriers within the channel.[30-31] It is worth noting that when NPs are incorporated with anisotropic structures-nanowires or nanorods, the NPs would be arranged in order within the nanowires to reduce a certain extent of Gibbs free energy.[32-33] Wherefore the electrospinning technique is not only a fabrication method, but also could be used as a simple and effective self-assembly method. Moreover, electrospinning usually does not require any surface functionalization process with costliness, it simply requires a suitable solvent with one kind of polymer dissolved in, and the NPs can be uniformly

dispersed in the solvent. However, no studies on the prepared STO/Fe_2O_3 nanowires by the electrospinning technique and their photodegradation activities for TC have been reported to date.

Herein, we firstly synthesized STO/Fe_2O_3 nanowires by a combination of hydrothermal and electrospinning method. First, STO nanoparticles (NPs) were successfully prepared via a facile hydrothermal method. Subsequently, different contents of STO NPs were formed on the Fe_2O_3 nanowires through an electrospinning technique. The as-prepared samples are employed as the photocatalyst to photodegrade TC under visible light. A series of STO/Fe_2O_3 photocatalytic activity is higher than both of the corresponding single component. In addition, to further detect the photocatalytic mechanism of photocatalysis process, the trapping experiment and ESR (Electron Spin Resonance) analysis were discussed in detail. This work demonstrates that the STO/Fe_2O_3 heterostructures provide performance of highly efficient for potential application in waste water treatment.

2. Experimental

2.1 Materials

Titania TiO_2 (P25) was purchased from Degussa (Germany). $Sr(OH)_2 \cdot 8H_2O$, KOH, $Fe(NO_3)_3 \cdot 9H_2O$ and ethanol were purchased from Aladdin (Shanghai, China). All the reagents are analytical grade and used without further purification and deionised water is used in the study. The experimental procedure is shown in Fig. 1.

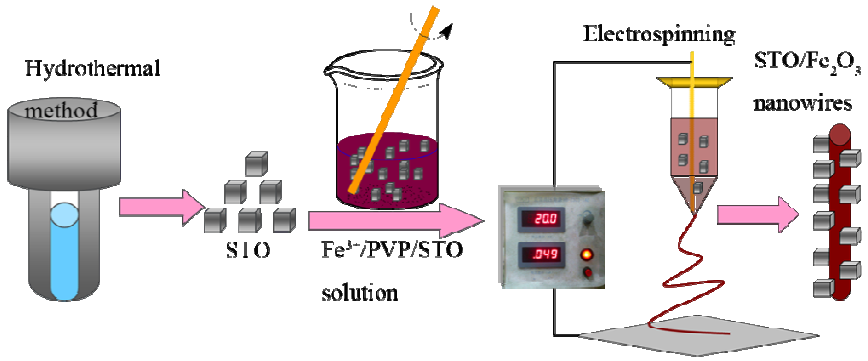

Fig. 1 Synthesis strategy to STO/Fe_2O_3 composite.

2.2 Catalysts synthesis

Synthesis of STO NPs: the cubes of STO NPs were synthesized by a typical hydrothermal method: 6 mmol $Sr(OH)_2 \cdot 8H_2O$, 6 mmol P25 and 4.2 g KOH were mixed in 66 ml deionised water under vigorous stirring for 30min, and then the mixture solution was transferred to a 100 ml Teflon-lined stainless steel autoclave at 150°C for 72h. After natural cooling, the STO was collected by centrifugation and washed with deionized water and ethanol until the pH of filtrate reached 7, and then dried at 60°C overnight in the vacuum oven.

Synthesis of STO/Fe_2O_3 nanowires: 0.606 g of $Fe(NO_3)_3 \cdot 9H_2O$ was dissolved in 7.5 mL of deionized water and 2.5 mL of ethanol, then 1.3g poly-(vinlypyrrolidone) and different mass of the as-prepared cubes STO NPs were mixed and dispersed by stirring for 6 h. Then the mixed solution was transferred into a syringe with a 5# stainless needle whose inner diameter was about 0.34 mm. The syringe was connected to a high-voltage generator (HB-Z303, China). In a typical experiment, a voltage of 18 kV was applied between the cathode (a metal collector) and the applied electric voltage was 20 kV with the spacing of 20 cm and the anode (needle) with the spacing of 20 cm. As-prepared composite PVP/$Fe(NO_3)_3$•$9H_2O$/STO nanofiber film was calcined at 500 °C for 2h under flow of N_2 gas for removing polymer and impurities. Finally, the STO/Fe_2O_3 composites were obtained by simply adjusting the usage of STO and were labeled as x-S/F, in which x refers to the STO theory loading amount

(x-S/F = 0.24-S/F, 0.30-S/F, 0.34-S/F, 0.4-S/F, 0.48-S/F).

2.3. Characterization

To determine the crystal phase of the obtained samples, powder X-ray diffraction (XRD) patterns were obtained on a D/MAX-2500 diffractometer (Rigaku, Japan) using Cu Kα radiation source (λ= 1.54178 Å) at a scan rate of 5° min^{-1}. Energy dispersive X-ray spectra (EDX) images were collected on an F20 S-TWIN electron microscope (Tecnai G2, FEI Co.), using a 200 kV accelerating voltage. Scanning electron microscopy (SEM) images were collected on an S-128 4800 field emission SEM (FESEM, Hitachi, Japan). Transmission electron microscopy (TEM) and high-resolution TEM (HRTEM) also had been used to characterize the samples. UV–vis diffused reflectance spectra (UV-vis) of the samples were obtained from a UV2550UV–vis spectrophotometer (Shimadzu, Japan). $BaSO_4$ was used as a reflectance standard. X-ray photoelectron spectroscopy (XPS) data were obtained by a Thermo ESCALAB 250X (America) electron spectrometer using 150 W Al Kλ radiations. The photoluminescence properties of the obtained samples were measured on a Perkin-Elmer LS 55 luminescence spectrometer. Total organic carbon (TOC) analyses were conducted on a multi N/C 2100 (Analytik Jena AG, Germany) TOC analyzer. The chemiluminescence intensity was measured using a Peltiercooled photon-counter head (Hamamatsu Photonics, H7421). The chemiluminescence analysis was measured using a Peltiercooled photon-counter head (Hamamatsu Photonics, H7421). Electron spin resonance (ESR) analysis was performed from a Bruker EPR A300-10/12 spectrometer.

2.4. Photocatalytic degradation of TC

TC was selected as a typical antibiotic to evaluate the photocatalytic degradation efficiency of the as-prepared photocatalysts under visible light. 0.1 g photocatalyst was added to 100 mL of tetracycline solution (10mg/L) with strong stirring to form a suspension. In order to rule out the effect of adsorption, the suspension was continuously stirred without irradiation for 30 min. A 250 W Xe lamp equipped with a

filter to cut off light of wavelength <420 nm was used as the light source. The supernatant liquid was sampled in 10 min interval and centrifuged (10,000 rpm, 5 min) to remove the photocatalyst particles. The concentration of aqueous TC was analyzed by the UV-vis spectrometer at 357 nm. The photocatalytic degradation ratio (DR) was calculated by the following formula:

$$TC_{DR} = \frac{A_0 - A_i}{A_0} \times 100\% \quad (1)$$

Where A_0 is the initial absorbance of TC, while A_i is the absorbance after illumination time *i*.

3. Results and discussion

3.1. Composition and Structure of as-prepared photocatalysts

X-ray diffraction (XRD) was used to investigate the phase composition, purity, and crystallinity of the resulting products. Before the measurement, the sample powders (15 mg) were pressed on the glass plate and then put into the D/MAX-2500 diffractometer. Fig. 2a shows the XRD diffraction patterns of Fe_2O_3 nanowires, STO NPs, and STO/Fe_2O_3 nanowires. According to the data in Fe_2O_3 JCPDS card (ICDD PDF#33-0664)[34] and $SrTiO_3$ JCPDS card (ICDD PDF#35-0734)[25], all the diffraction lines in Fig. 2 can be assigned to the hematite Fe_2O_3 nanowires and cubes STO NPs. There are no other impurity diffraction lines are discovered, which revealed that we have successfully synthesized highly stable and crystalline STO/Fe_2O_3 nanowires with this method and confirm the purity of the product.[35] The energy dispersive X-ray spectrum (Fig. 2b) contains the elements of Sr, Ti, O and Fe in the STO/Fe_2O_3 nanowires.

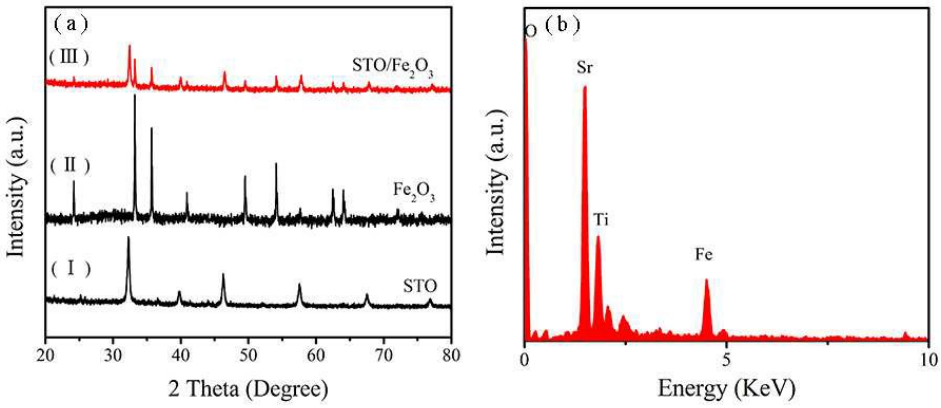

Fig. 2 (a) X-ray diffraction patterns of cubic STO NPs (I), hematite Fe_2O_3 (II), and Fe_2O_3/STO (III); (b) EDX spectrum of Fe_2O_3/STO nanowires.

The surface morphology and particle size of the representative photocatalysts were performed by the typical electron microscope images. 5mg of samples were dispersed into 5mL of ethanol and ultrasonically treated for 10 min. Then a certain amount of suspension was dript to the copper net and oven dried under the infrared lamp. Take the prepared sample into the equipment. Analyses of SEM images are depicted in Fig. 3. As shown in Fig. 3a, average diameter of Fe_2O_3 nanowires is about 200 nm. From the Fig. 3b, the STO NPs is layout of the surface of Fe_2O_3 nanowires by electrospinning method and the composite have partial reunion. For comparison, transmission electron microscopy (TEM) provides insights into the structure of Fe_2O_3 nanowires, STO NPs, and STO/Fe_2O_3 nanowires. Fig. 3c shows the TEM image of the parent Fe_2O_3 nanowires, where the prepared Fe_2O_3 nanowires appear to be smooth on the surface without STO NPs. Fig. 3d presents the TEM image of STO NPs obtained after hydrothermal treatment. One can notice that the sample was composed of nanocubes with a mean size of 50 nm. Fig. 3e shows that STO nanocubes have been densely grown on the Fe_2O_3 nanowires after the electrospinning process, which is

beneficial to the interparticle photo-induced carriers transfer. The crystalline nature of the NPs was confirmed by lattice fringes. The aggregation of particles was evident from HRTEM image, as shown in Fig. 3f. The lattice fringe spacing of 0.27 nm and 0.276 nm are consistent with the interplanar distances of (104) plane of Fe_2O_3 nanowires and (110) plane of STO NPs.[25]

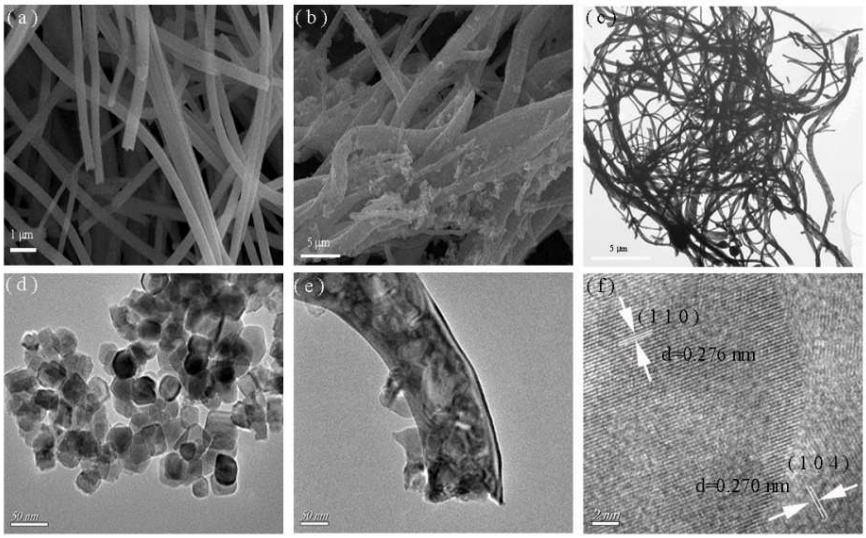

Fig. 3 SEM images of pure (a) Fe_2O_3 nanowires and (b) STO/Fe_2O_3 nanowires; TEM images of pure (c) Fe_2O_3 nanowires, (d) STO nanocubes and (e) STO/Fe_2O_3 nanowires; (f) HRTEM images of STO/Fe_2O_3 nanowires.

The XPS spectra were recorded to determine the oxidation state and electronic environment of the elements. The XPS data were obtained with a Thermo ESCALAB 250Xi (America) electron spectrometer using 150 W Al Kα monochromatic light radiations. The beam spot is 500μm and the binding energies were referenced to the C1s line at 284.8 eV from adventitious carbon. The experimental procedure was prepared as follows: the powder sample was spread on the conductive adhesive tape to form a tight face and the loose powders was blew off by washing ear ball; then put the sample into the equipment, picked up the suction, chose to scan area, scanning and save data. The full range XPS survey spectrum of 0.34-STO/Fe_2O_3 nanowires is illustrated in Fig. 4a and Fig. 4b–e shows the core level spectra of characteristic elements. The peaks occurred at 711 eV and 724.5 eV were due to Fe 2p3/2 and Fe

2p1/2 of Fe_2O_3 nanowires respectively.[36] The same values have been reported in the literature.[37-38] Hence, the oxidation state of Fe in 0.34-STO/Fe_2O_3 nanowires was established to be +3. The peaks at 458.2 eV and 463.6 eV belong to Ti 2p3/2 and Ti 2p1/2 states respectively, which are assigned to Ti^{4+} from STO. And in the Fig. 4c, two strong peaks centered at 132.8 eV and 134.9 eV are is ascribed to Sr $3d_{5/2}$ and Sr $3d_{3/2}$ states, respectively, which implies that the main elemental chemical states are divalent and bands with titanates.[25] Thus XPS spectra confirmed the presence of Ti, Fe, O and Sr in the material. From Fig. 4f, it can be found that the peak of binding energy for Fe 2p3/2 is composed of 711.0 and 709.1 eV, which are assigned to Fe^{3+} and Fe^{2+} ions, respectively.[39,40] The formation of Fe^{2+} in the 0.34-STO/Fe_2O_3 nanowires would be ascribed to the photoinduced interfacial charge transfer (IFCT): the electrons from the VB of STO NPs to the Fe_2O_3 nanowires, and the becomes to Fe^{2+}.

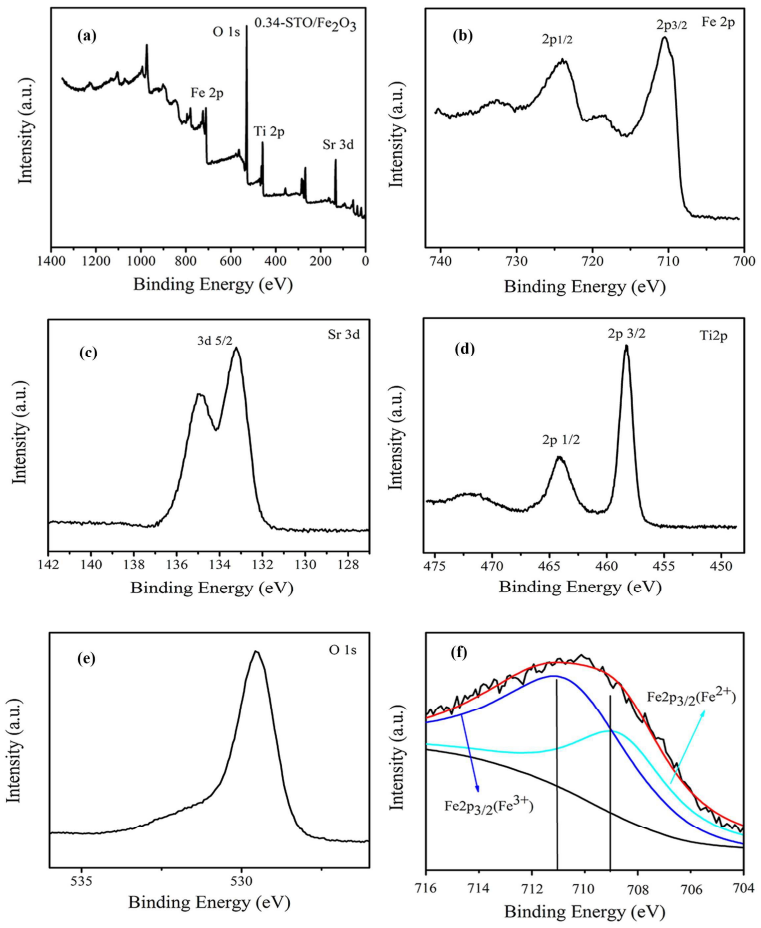

Fig. 4 (a) The full range XPS spectrum; (b-e) the high-resolution XPS spectra of Fe, Sr, Ti and O respectively of 0.34-STO/Fe_2O_3 nanowires; (f) high-resolution XPS spectra of Fe2p3/2 region for the 0.34-STO/Fe_2O_3 nanowires under visible light irradiation for 140 min

3.2. Optical properties of as-prepared photocatalysts

UV−vis spectroscopy is one of the most important analytical tools for characterizing the optical properties of materials. The UV−vis absorption spectra of as-synthesized samples in the pressed disk form were recorded on a Shimadzu UV-2500 spectrophotometer equipped with an integrating sphere assembly, over a wavelength range of 200−700 nm employing $BaSO_4$ as a reflectance standard. The pressed disk is compose by $BaSO_4$ powders and as-synthesized samples: $BaSO_4$ powders were flatted on the diffusion reflective cell, went its level planish again, 50mg as-synthesized samples were planished on the center of diffusion reflective cell. Fig. 5 shows the results of UV−vis diffuse reflectance spectra of STO NPs, Fe_2O_3 nanowires, and 0.34-STO/Fe_2O_3 nanowires. The characteristic absorption of STO exhibited a spectrum with a sharp absorption edge at 400 nm, which corresponds to band gap energy of 3.2 eV, $\lambda=1240/Eg$. The result indicates that STO NPs almost had no absorption in the visible light range ($\lambda<400$ nm). The spectrum of Fe_2O_3 nanowires showed a high energy absorbance peak at 550 nm and with the participation of Fe_2O_3 nanowires, the STO/Fe_2O_3 nanowires absorption band edge is extended to 550 nm, which implies that this method can overcome the lack of visible light response of STO NPs. We can also observe a color change of the samples, that is, from white to

red-brown (inset in Fig. 5, the pure STO NPs is white, and 0.34-STO/Fe_2O_3 nanowires is red-brown). It is well known that with wide band gap of 3.2 eV, STO NPs only absorbs the ultraviolet light ($\lambda < 400$ nm).[17] Fe_2O_3 nanowires is also a semiconductor with a band gap of 2.3 eV, whose absorption wavelength corresponds to 540 nm. Therefore, due to the inherent characteristics of these two semiconductors, 0.34-STO/Fe_2O_3 nanowires had intensive absorption in the visible light range (550nm).

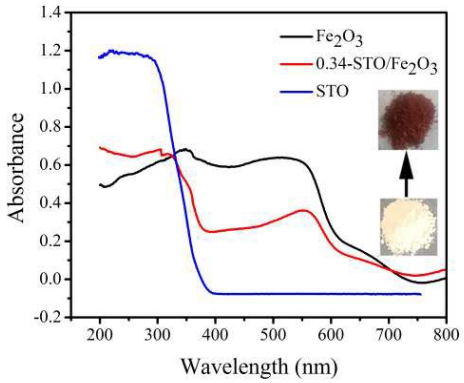

Fig. 5 UV-vis diffuses reflectance spectra of different samples with color contrast in photos (inset).

3.3. Photocatalytic activity of as-prepared photocatalysts

As shown in Fig. 6, the catalytic activities of the pure STO NPs, Fe_2O_3 nanowires and a series of STO/Fe_2O_3 samples were carried out in 140 min under visible light irradiation ($\lambda > 420$ nm) for comparison. According to the results, we can intuitively notice that degradation rate of pure STO NPs is inappreciable because it only possesses activity under UV light. The pure Fe_2O_3 nanowires reveal feeble photocatalytic performance for degrading TC under visible light irradiation, which is far from meeting the requirements of industrialization. Conversely, the STO/Fe_2O_3 nanowires show excellent enhancement in the photodegradation of TC (DR=33.3%)

under visible light irradiation. As shown in Fig. 6b, with 0.24g STO NPs participating, 0.24-STO/Fe_2O_3 nanowires showed slightly higher activity than pure STO NPs and Fe_2O_3 nanowires, with the DR enhancing to 61.2%. With the proportion of STO NPs increasing, the 0.34-STO/Fe_2O_3 nanowires shows the highest DR of 82.7%. However, the photocatalytic degradation activity decreases rapidly as the concentration of STO NPs exceeds 0.34g. The lowest rate of photocatalytic degradation of TC is 66.8% (0.48-STO/Fe_2O_3 nanowires), but it is still much higher than that of the STO NPs (8.5%) and Fe_2O_3 (33.3%) nanowires. It demonstrates that the STO NPs loading amount forcefully affects the photocatalytic activity. Meanwhile, this photocatalyst provides an effective pathway to solve the environmental pollution.

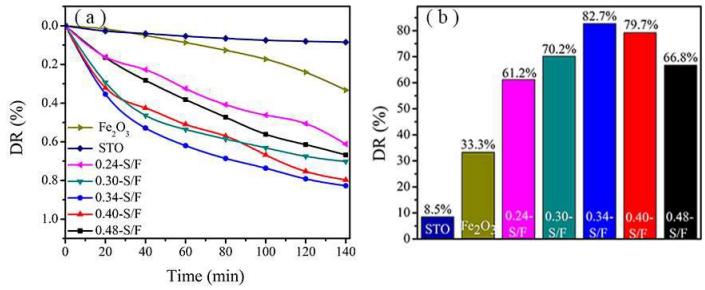

Fig. 6 (a) Photocatalytic activity towards the degradation of TC with as-prepared samples under visible light irradiation; (b) photocatalytic degradation ratios of TC after 140 min.

3.4. The kinetic study of photocatalytic degradation of TC

Fig. 7a shows the photodegradation of TC on different photocatalysts fits pseudo-first-order kinetics, [41] $\ln(C_0 / C) = k_{app} t$, where C is the concentration of TC (mg/L) at time t, and C_0 is the initial concentration at t= 0. k_{app} denotes the degradation rate constant and it enables one to determine a photocatalytic activity. The rate constant and the intercept were given in Fig. 7b, and the value of k_{app} gives an

indication of the photodegradation activity of the photocatalysts. It can be visually seen in Fig. 7 that 0.34-STO/Fe_2O_3 nanowires exhibits the highest photodegradation activity, with the maximum degradation rate constant of about 0.0117 min^{-1}, which is consistent with the result of the photocatalytic degradation of TC under visible light.

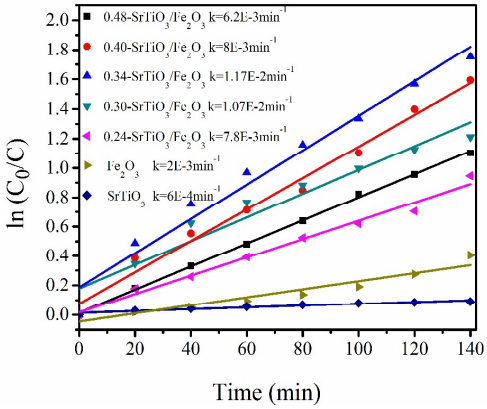

Fig. 7 The first-kinetic of the photocatalytic degradation of TC over different photocatalysts in 140 min under visible light irradiation.

3.5. Photoluminescence spectra (PL) analysis of as-prepared photocatalysts

Photoluminescence (PL) analyses were conducted on different samples. It is well acknowledged that the PL emission intensity is related to the recombination of electrons and holes. The lower PL emission intensity shows the less of an opportunity for electron-hole pairs' recombination, the more effectively migration of charge-carriers, thereby.[41] Before the measurement, samples (10 mg) were well-dispersed into 5 mL of ethanol, and the measurement was conducted at the excitation wavelength of 325 nm with PMT voltage of 500 V and the PL emission maximum of samples are at 430 nm. As shown in Fig. 8, the PL emission intensity were found to be in the order of STO NPs > Fe_2O_3 nanowires > 0.34-STO/Fe_2O_3 nanowires, which is the exact reverse order of DR. The completely opposite data of PL and DR sufficiently demonstrate the STO/Fe_2O_3 nanowires has a lower

recombination of photoinduced electron-hole pairs, when the recombination rate decreases, more photo-generated charge carriers can participate in the photochemical transformation, resulting in the enhancement of photocatalytic activity.

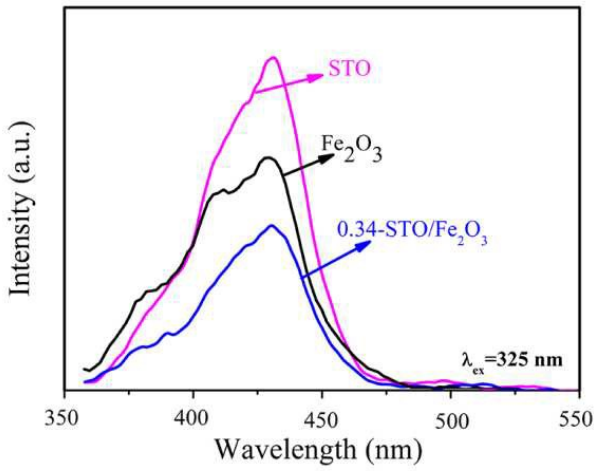

Fig.8 PL spectrum of different samples with the excitation wavelength of 325 nm.

3.6. Total organic carbon (TOC) analyses of photocatalytic degradation of TC

In order to demonstrate that reduced concentrations of tetracycline is from photocatalytic degradation rather than from other effects, TOC analyses were conducted.[42] As shown in Fig. 9a, the reduction of TC with the photocatalyst of the 0.34-STO/Fe_2O_3 nanowires under visible light is reached 49.8%, which is much lower than that of the photocatalysis. And the Fig. 9b gives specific comparison between photodegradation rate and TOC removal. After irradiation under visible light for 20min, the photodegradation rate is 35.4% with 0.34-STO/Fe_2O_3 nanowires (Right oblique map), but the value of TOC is 17.7% (Left oblique map). As the time going, the photodegradation rate reach 82.7% finally, and the value of TOC is less than that, reaching 49.8%. The reasonable reason is that there may be some small organic

molecule generated in the process. While similar trends of TOC removal and the degradation curves correctly illustrates our experiments of photodegradation successfully removed the effect of physical adsorption. Meanwhile, the trend of the TOC means our photocatalysts have enormous potential of decomposition of TC.

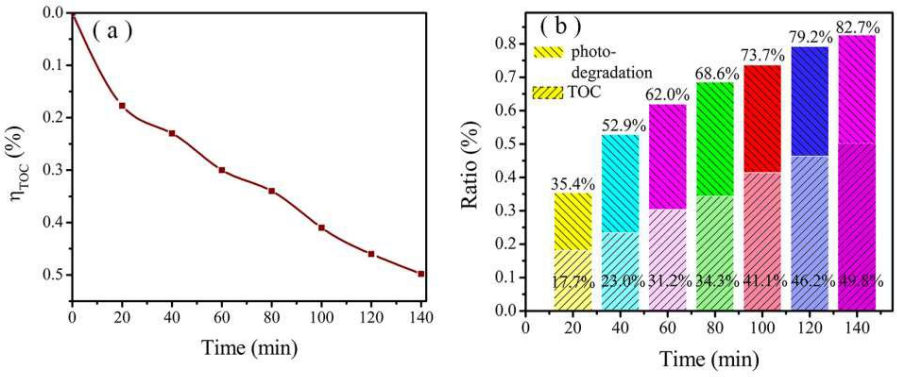

Fig. 9 (a) TOC removal curves of 0.34-STO/Fe_2O_3 under visible light irradiation; (b) photo-degradation curve trend contrasts TOC in 140 min.

3.7. The photocatalytic stability and repeatability of as-prepared photocatalysts

To evaluate the stability and repeatability of the photocatalytic performance of the 0.34-STO/Fe_2O_3 nanowires, four consecutive cycles photocatalytic degradation of TC were performed, using the same photocatalyst and a fresh TC solution in each time. The results of the cycling experiments are depicted in Fig. 10b. It exhibits that the photocatalytic activity of 0.34-STO/Fe_2O_3 nanowires has a tiny deactivation in the photodegradation of TC, which may originate from the unavoidable loss of the photocatalyst by centrifugation. Furthermore, the stability was detected by using XRD of the photocatalyst before and after the photocatalytic recycles. As shown in Fig. 10a, there are no observation of additional peaks related to FeO specie and the XRD diffraction patterns of 0.34-STO/Fe_2O_3 nanowires have almost no change after

photocatalytic cycles, implying that 0.34-STO/Fe_2O_3 nanowires is photostable. Hence, 0.34-STO/Fe_2O_3 nanowires may serve as one of the promising candidates for application in purification of antibiotic waste water.

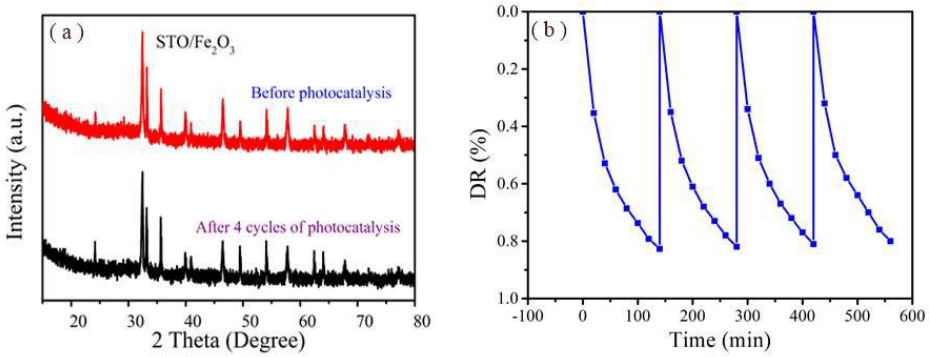

Fig. 10 (a) XRD patterns of 0.34-STO/Fe_2O_3 before and after photocatalytic reaction and (b) Four reaction cycles for the phtotcatalytic degradation of TC by 0.34-STO/Fe_2O_3.

3.8 Reactive species in the catalytic system

To further investigate the active species in photodegrading TC, a series of active species trapping experiments were conducted. Fig. 11 shows the results of adding a series of quenchers over the 0.34-STO/Fe_2O_3 nanowires to determine the dominant oxidative species in the photocatalytic process, namely, triethanolamine (TEA), iso-propanol (IPA) and $AgNO_3$. When TEA traps for h^+ is added into the reaction system, the photodegradation is significantly inhibited compared to the reaction without radical scavengers,[43-47] which confirms the paramount role of h^+ in the reaction process. An obvious suppression phenomenon is also happened when IPA was addicted for scavenging ·OH,[48] but not as much as IPA did. The importance of the activated species follows the order: h^+ >·OH. On the contrary, the photocatalytic degradation of TC obviously increased with the addition of $AgNO_3$[43-47] for e^-. The increase suggests that the scavenger of e^- has less of an opportunity for electron-hole pairs' recombination and facilitates the production of more holes. This result fully

confirmed that the degradation of TC over 0.34-STO/Fe_2O_3 nanowires is driven mainly by the participation of h^+, secondary by ·OH.

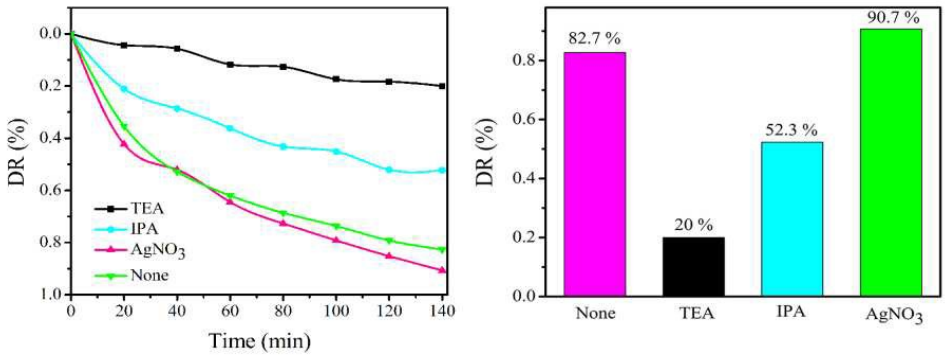

Fig. 11 (a) Photocatalytic degradation ratios of TC using different radical scavengers over 0.34-STO/Fe_2O_3 nanowires under visible light irradiation for 140 min, (b) photocatalytic degradation ratios of TC after 140 min.

To further verify the generation of radicals ($•O_2^-$ and •OH), the ESR (Electron Spin Resonance) of 0.34-STO/Fe_2O_3 nanowires was proceeded using dimethyl pyridine N-oxide (DMPO) as trapping agent. At first, the 0.34-STO/Fe_2O_3-CH_3OH-DMPO and 0.34-STO/Fe_2O_3-H_2O-DMPO were prepared by the following process: 10 mg samples were dissolved in 0.5 mL deionized water and 30μL 5,5-dimethyl-1-pyrrolineN-oxide (DMPO) with ultrasonic for 10 min (solution A) and the solution B were prepared the same except the CH_3OH replaced by water. Hydroxyl radicals (DMPO-·OH) is detected by the solution A, and solution B was for the superoxide radicals (DMPO-·O_2^-). As shown in Fig. 12a, it can be seen that the strong characteristic peaks with the peak height ratio is 1: 2: 2: 1 corresponding to DMPO-·OH adducts and in Fig. 12b, the characteristic peaks with the peak height ratio is 1: 1: 1: 1 were assigned to the DMPO-·O_2^- adducts.[25] This proves that the ·O_2^- have been produced during the process of photocatalytic reaction. The number of characteristic peaks of the DMPO-·O_2^- adducts is four, this is because the solution B is neutral (PH=7). The

number will be six, while the solution is acid, and this is due to their hyperfine splitting peaks are not the same.[25] According to the active species trapping experiments and ESR analyses, we can make a possible conclusion that in addition to A and B, C also occupies a major position in the photocatalytic degradation of TC.

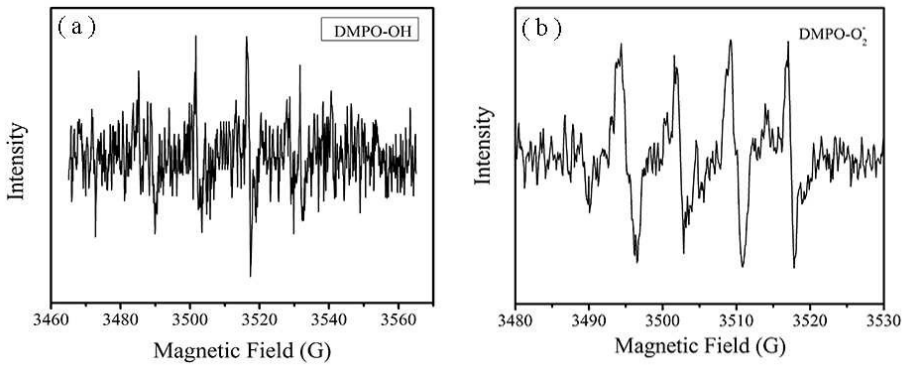

Fig. 12 DMPO spin-trapping ESR spectra of TC solutions after visible light irradiation: (a) 0.34-STO/Fe_2O_3-H_2O/DMPO, (b) 0.34-STO/Fe_2O_3-CH_3OH/DMPO.

3.9 Chemiluminescence analysis of as-prepared photocatalysts

The chemiluminescence analysis was measured using a Peltiercooled photon-counter head (Hamamatsu Photonics, H7421). Luminol chemiluminescence probe method was carried out to detect the generation of $\cdot O_2^-$. Before the measurement, the samples (15 mg) was added in 0.01 M NaOH solution (3.5 mL) in a quartz cell with the size of 1 cm × 1 cm. Then the suspension was irradiated under the visible light. After the irradiation, 7 mM luminol solution (50 μL) was immediately added in the suspension. The operational processes of measurements of H_2O_2 were the same as the $\cdot O_2^-$ measurement except for the injection solution and the timing. After the irradiation of the photocatalysts, the suspension was kept in dark to eliminate $\cdot O_2^-$. Then 7 mM luminol solution (50 μL) was added in the suspension, and the suspension was kept in the dark for 10min. 50 μL of hemoglobin (Hb) solution was added in the suspension, and then the chemiluminescence intensity was measured using the photon counter system described above.

Fig. 13 shows the concentrations of $\cdot O_2^-$ and H_2O_2 produced by the STO NPs and

0.34-STO/Fe_2O_3 nanowires under the irradiation of visible light. It is worth observing that pure STO NPs produce little H_2O_2 and $\cdot O_2^-$, this is maybe due to the visible light could not almost be absorbed and reaction can be ignored.

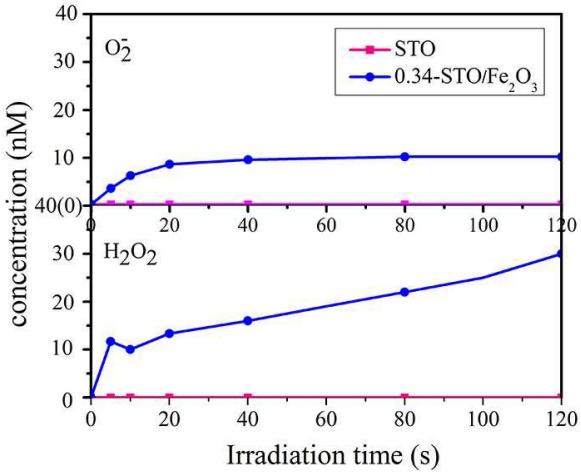

Fig. 13 The concentration of $\cdot O_2^-$ and H_2O_2 produced by visible light irradiation as a function of irradiation time for 0.34-STO/Fe_2O_3 nanowires.

In the 0.34-STO/Fe_2O_3 nanowires, $\cdot O_2^-$ and H_2O_2 were detected as seen in Fig. 13 and one can note that H_2O_2 grow faster than $\cdot O_2^-$, which indicates that the formed H_2O_2 was oxidized into $\cdot O_2^-$ within photocatalytic reaction. These experiment results imply that H_2O_2 was emerged by two-electron reduction of O_2 rather than generating $\cdot O_2^-$ by the one-electron reduction of O_2.[48] When electron has a potential energy of +0.695 V, it can reduce O_2 by two electrons into H_2O_2. So, the redox potential of Fe^{3+}/Fe^{2+} may be near to or more negative than +0.695 V.[49]

Recently, it was reported that due to the interfacial charge-transfer mechanism (IFCT) the metal oxides grafted titania showed visible light responsive photocatalytic activity.[48] A similar mechanism may be considered in STO/Fe_2O_3 nanowires system and the mechanism of photocatalytic reactions on visible-light irradiation is illustrated

in *Scheme 1*, which shows the redox potentials of STO NPs versus the standard hydrogen electrode potential. The interfacial charge transfer from the VB of STO NPs to Fe_2O_3 nanowires results in the enhanced absorption from~500 to 600 nm. The transferred electrons from the VB of STO NPs to Fe_2O_3 nanowires cause the partial reduction of Fe^{3+} to Fe^{2+}, which has been confirmed by the previous XPS results. The holes produced in the VB of STO NPs produces ·OH to degrade TC. Meanwhile, the O_2 react with Fe^{2+} to generate H_2O_2. So, h^+, H_2O_2 and ·OH had major roles in the photocatalytic degradation of TC. Consequently, this IFCT will retard the recombination of photoinduced electrons and holes due to space separation and degrade the TC. Thus, it is not surprising that when x is lower than 0.34 with increasing STO NPs are deposited on the surface of Fe_2O_3 nanowires, resulting in the increase of photodegradation activity because of more IFCT electrons produced. The major electron transfer steps in the above photocatalytic mechanism under visible light irradiation are summarized by the following equations (eq2-5):

$$STO / Fe_2O_3 + hv \rightarrow STO\left(h^+\right) / Fe_2O_3\left(e^-\right) \quad (2)$$

$$O_2 + 2e^- + 2H^+ \rightarrow H_2O_2 \quad (3)$$

$$H_2O_2 \rightarrow \cdot O_2^- + 2H^+ \quad (4)$$

$$h^+ + H_2O \rightarrow \cdot OH + H^+ \quad (5)$$

Conversely, with further increasing the content of STO NPs (>0.34g), STO NPs will shield the incident light resulting in the lower photocatalytic activity.

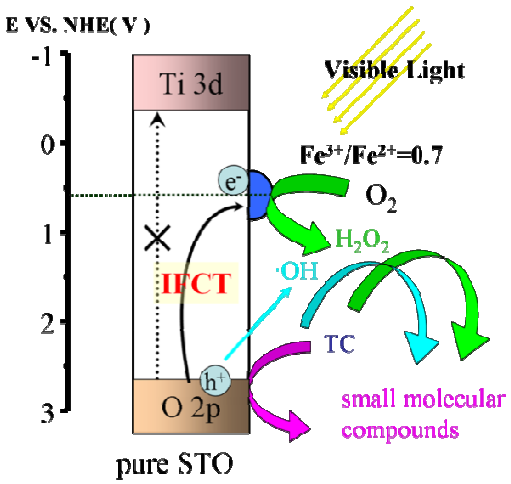

Scheme 1 Mechanistic pathway of electrons and holes under visible light illumination over 0.34-STO/Fe_2O_3 nanowires.

4. Conclusion

In summary, $SrTiO_3/Fe_2O_3$ nanowires are prepared for the first time via electrospinning-assisted hydrothermal synthesis. The prepared $SrTiO_3/Fe_2O_3$ nanowires show especially higher visible light photodegrading tetracycline than pure $SrTiO_3$ nanoparticles and Fe_2O_3 nanowires. Meanwhile, the photocatalytic activity is strongly influenced by the amount of $SrTiO_3$ nanoparticles loading content and the theory loading amount is at 0.34 had the highest photodegradation of tetracycline, reaching 82.7%. It is believed that visible light irradiation induces the direct interfacial charge transfer from the valence band of $SrTiO_3$ nanoparticles to Fe_2O_3 nanowires. This work shows a possibility for replacing noble metal catalysts by economical Fe_2O_3 in the photodegradation of antibiotic.

Acknowledgments

We gratefully acknowledge the financial support of the National Natural Science Foundation of China (21546006, 21276116, and 21477050), Excellent Youth Foundation of Jiangsu Scientific Committee (BK20140011), Chinese-German Cooperation Research Project (GZ1091). Henry Fok Education Foundation (141068)

and Six Talents Peak Project in Jiangsu Province (XCL-025 and XNY-009). The Start-Up Foundation of Jiangsu University (11jdg104) and the Natural Science Foundation of Jiangsu Province (BK20150536).

References

1 H. W. Peng, S. Y. Pow, T. L. Teik, *Appl. Catal. A: Gen.,* 2011, **399,** 252-261.

2 B. L. Yan, J. G. Xiao, X. Z. Bao, T. X. Bi, H. L. Jin, P. D. Chao, B. Jing, M. C. Wei, *J. Hazard. Mater.,* 2009, **171**, 678-683.

3 N. Y. Xiu, Y. L. Zi, H. Ming, T. C. Ting, D. S. Wei, W. H. Peng, S. Y. Yong, X. F. Yu, Reac. Kinet, *Mech. Cat.,* 2014, **111**, 347-360.

4 D. Z. Xiang, J. W. Yu, J. S. Rui, M. Z. Dong, *Chemosphere*, 2013, **92**, 925-932.

5 C. Reyes, J. Fernandez, J. Freer, M.A. Mondaca, C. Zaror, S. Malato, H.D. Mansilla, *J. Photoch. Photobio. A*, 2006, **184**, 141-146.

6 F. W. Xiao, F. W. Yuan, X. Z. Jia, Z. Xin, K. Z. Wei, *Bioresource. Technol.*, 2011, **102**, 5924-5931.

7 H. Rong, X. Xin, X. Z. Xiao, M. N. Jun, D. Z. Wei, *J. Hazard. Mater.*, 2012, **209-210**, 137-145.

8 L. L. Xin, L. Peng, X. Y. Guan, C. M. Chang, W. H. Peng, S. Y. Yong, *Chem. Eng. J.*, 2013, **217**, 398-406.

9 F. D. S. Luís, C. M. Jean, A. Juan, B. Armando, G. Lourdes, I. B. B. Maria, M. Alexandre, A. Eduardo, L. M. Mário, R. M Valmor, *J. Phys. Chem. C*, 2014, **118**, 4930-4940.

10 M. Yu, S. Zhao, H. Wu, S. Asuha, *J. Porous. Mater.*, 2013, **20**, 1353-1360.

11 P. Tarawipa, S. Thammanoon, Y. Susumu, C. Sumaeth, *J. Mol. Catal. A: Chem.*,

2008, **287**, 70-79.

12 L. Min, Q. Q. Xiao, M. Masahiro, H. Kazuhito, *J. Am. Chem. Soc.*, 2013, **135**, 10064-10072.

13 H. L. Jin, B. L. Shu, B. L. Yan, B. Jing, X. Z. Bao, F. H. Xiao, *J. Hazard. Mater.*, 2013, **262**, 482-488.

14 H. X. Tai, Y. S. Xiao, L. Jun, *J. Phys. Chem. C*, 2008, **112**, 9753-9759.

15 G. Y. Huo, I. Hiroshi, S. Yoshiki, H. Yasuhiro, K. Yasushi, M. Masahiro, H. Kazuhito, *J. Phys. Chem. C*, 2011, **114**, 16481-16487.

16 T. Hua, Z. Du, G. T. Guo, R. J. Xiao, J. L. Wen, S. L. Chang, F. Y. Xiao, *Ceram. Int.*, 2013, **39**, 8633-8640.

17 K. Guo, Z.F. Liu, Y. Wang, Y.F. Zhao, Y.C. Xiao, J.H. Han, Y.J. Li, B. Wang, T. Cui *Int. J. Hydrogen. Energ.*, 2014, **39**, 13408-13414.

18 L. Wang, Z.J. Wang, D.H. Wang, X.C. Shi, H. Song, X.Q. Gao, *Solid State Sci.,* 2014, 31, 85-90.

19 J. Zhou, L. Yin, H.R. Li, Z.Y. Liu, J.X. Wang, K. Duan, S.X. Qu, J. Weng, B. Feng, *Mat. Sci. Semicon. Proc.,* 2015, **40**, 107–116.

20 P. Z. Jian,; Z. Z. Long, L. L. Sheng, H. L. Le, B. L. Xu, J. Z. Ming, L. Yan, C. G. Guo, *Int. J. Hydrogen. Energ.*, 2012, **37**, 17068-17077.

21 Z. Wu, Y.F. Su, J.D. Yu, W. Xiao, L. Sun, C.J. Lin, *Int. J. Hydrogen. Energ.*, 2015, **40**, 9704-9712.

22 H. C. Chen, C. W. Huang, C. S. Jeffrey, S. T. Lin, *J. Phys. Chem. C*, 2012, **116**, 7897-7903.

23 H.W. Bai, J. Jermyn, Z. Y. Liu, X. X. Song, S. L. Siew, D. S. Darren, *Appl. Catal. B: Environ.*, 2012, **125**, 367-374.

24 X. Chen, P.F. Tan, B.H. Zhou, H.G. Dong, J. Pan, X. Xiong, *J. Alloy. Compd.,* 2015, **647**, 456-4622012.

25 P. Li, B. L. Chun, L. W. Guo, H. Yang, L. Shuang, R. Ao, H. L. Ke, S. X. Li, D. S. Wei, *RSC Adv.*, 2014, **4**, 47615-47624.

26 A. Rikako, N. Hiroaki, X. J. Qing, J. S. Ken, Iw. Akihide, Ku. Akihiko, *Chem. Commun.*, 2014, **50**, 2543-2546.

27 J. G. Jian, X. O. Shu, L. Peng, J. Z. Yuan, K. Tetsuya, H. Y. Jin, *Appl. Catal. B: Environ.,* 2013, **134**, 286-292.

28 M. Liu, C. R. M, G. Collins, J. Liu, C. L. Chen, C. Dai, S. Li, X. Feng, W. Hong, H. Jie, C. J. Jie, I. M. Efstathios, W. C. Melanie, *ACS Appl. Mater. Interfaces,* 2012, **4**, 5761-5765.

29 W. H. Hung, T. M. Chien, C. M. Tseng, *J. Phys. Chem. C*, 2014, **118**, 12676-12681.

30 S. H. Choi, B. H. Jang, J. S. Park, De. Renaud, L. T. Harry, K. Doo, *Acs Nano.*, 2014, **8,** 2318-2327.

31 C. F. Jie, L. Z. Jun, H. Z. Chang, P. Yong, D. L. Xiao, M. H. Yong, X. Z. Zhen, J. P. Xiao, J. M. Nigel, Q. X. Er, *J. Alloy. Compd.*, 2013, **577**, 97-102.

32 C.L. Zhang, K. P. Lv, H.P. Cong, S.H. Yu, *Small*, 2012, **8**, 647-653.

33 K. Frank, G. Yury, A. Ashraf, N. Nevin, H.Y. Hai, L.Y. Guo, L. Christopher, W. Peter, *Adv. Mater.*, 2013, **15**, 161-1165.

34 C. L. Zhu, H. L. Yu, Z. Yue, T. S. Wang, Q. Y. Ouyang, L. H. Qi, Y. J. Chen, X. Y. Xue, *ACS Appl. Mater. Interfaces*, 2014, **4**, 665-671.

35 Z. Lou, F. Li, J. N. Deng, L. L. Wang, T. Zhang, *ACS Appl. Mater. Interfaces*, 2013, **5**, 12310-12316.

36 B. Palanisamy, C. M. Babu, B. Sundaravel, S. Anandan, V. Murugesana, *J. Hazard. Mater.*, 2013, **252-253**, 233-242.

37 Y. Toru, H. Peter, *Appl. Surf. Sci.*, 2008, **254**, 2441-2449.

38 G. Bhargava, I. Gouzman, C. M. Chun, T. A. Ramanarayanan, S. L. Bernasek, *Appl. Surf. Sci.*, 2007, **253**, 4322-4329.

39 T. H. Xie, X. Y. Sun, J. Lin, *J. Phys. Chem. C*, 2008, **112**, 9753-9759.

40 Q. Liu, Y.R. Guo, Z.H. Chen, Z.G. Zhang, X.M. Fang, *Appl. Catal. B: Environ.,* 2016, **183**, 231-241.

41 G. H. Zhang, W. S. Guan, H. Shen, X. Zhang, W. Q. Fan, C. Y. Lu, H.Y. Bai, L. S. Xiao, W. Gu, W. D. Shi, *Ind. Eng. Chem. Res.*, 2014, **53**, 5443-5450.

42 Y. Yan, Y. F. Wu, Y. T. Yan, W. S. Guan, W. D. Shi, *J. Phys. Chem. C*, 2013, **117**, 20017-20028.

43 S. C. Yan, Z. S. Li, Z. G. Zou, *Langmuir*, 2010, **26**, 3894-3901.

44 S. Q. Liu, N. Zhang, Z. R. Tang, Y. J. Xu, *ACS Appl. Mater. Interfaces*, 2012, 4, 6378-6385.

45 X. C. Wang, M. Kazuhiko, X. F. Chen, T. Kazuhiro, D. Kazunari, Y. D. Hou, X. Z. Fu, A. Markus, *J. AM. Chem. Soc.*, 2011, 131, 1680-1681.

46 L. Q. Ye, J. Y. Liu, C. Q. Gong, L. H. Tian, T. Y. Peng, L. Zan, *ACS Catal.*, 2012, 2,

1677-1683.

47 T. B. Li, G. Chen, C. Zhou, Z. Y. Shen, R. C. Jin, J. X. Sun, *Dalton Trans.*, 2011, 40, 6751-6758.

48 N. Masami, M. Yasufumi, N. Yoshio, *J. Phys. Chem. C*, 2012, 116, 14900-14907.

49 N. Yoshio, T. Shinichiro, S. Hodaka, Y. N. Atsuko, *J. Phys. Chem. C*, 2011, 115, 21283-21290.

Gaphical Astract

TEXT: Visible light irradiation can induce carrier transfer and generate oxidizing species of $SrTiO_3/Fe_2O_3$ nanowires to degrade tetracycline.

GRAPHIC: